Calcium-driven regulation of voltage-sensing domains in BK channels

Yenisleidy Lorenzo-Ceballos[1,2], Willy Carrasquel-Ursulaez[2], Karen Castillo[2], Osvaldo Alvarez[2,3] and Ramon Latorre[2 (*)]

[1]Doctorado en Ciencias Mención Neurociencia, Facultad de Ciencias, Universidad de Valparaíso, Valparaíso, Chile; [2]Centro Interdisciplinario de Neurociencia de Valparaíso, Facultad de Ciencias, Universidad de Valparaíso, Valparaíso, Chile; [3]Departamento de Biología, Facultad de Ciencias, Universidad de Chile, Santiago, Chile.

(*) Correspondence and Requests for materials should be addressed to Ramon Latorre (ramon.latorre@uv.cl)

Abstract

Allosteric interplays between voltage-sensing domains (VSD), Ca^{2+}-binding sites, and the pore domain govern the Ca^{2+}- and voltage-activated K^+ (BK) channel opening. However, the functional relevance of the Ca^{2+}- and voltage-sensing mechanisms crosstalk on BK channel gating is still debated. We examined the energetic interaction between Ca^{2+} binding and VSD activation measuring and analyzing the effects of internal Ca^{2+} on BK channels gating currents. Our results indicate that the Ca^{2+} sensors occupancy has a strong impact on the VSD activation through a coordinated interaction mechanism in which Ca^{2+} binding to a single α-subunit affects all VSDs equally. Moreover, the two distinct high-affinity Ca^{2+}-binding sites contained in the C-terminus domains, RCK1 and RCK2, appear to contribute equally to decrease the free energy necessary to activate the VSD. We conclude that voltage-dependent gating and pore opening in BK channels is modulated to a great extent by the interaction between Ca^{2+} sensors and VSDs.

Introduction

Diverse cellular events involve calcium ions as a primary mediator in the signal transduction pathways triggering, among other signaling processes, Ca^{2+}-activated conductances. Since the BK channels are regulated by cytosolic Ca^{2+} and depolarizing voltages (Marty, 1981; Pallotta et al., 1981; Latorre et al., 1982), they are integrators of physiological stimuli including intracellular Ca^{2+} elevation and membrane excitability. BK channels are modular proteins where each module accomplishes a specific channel function. Thus, different modules harbor voltage and Ca^{2+} sensors that communicate with the channel gate allosterically (Cox et al., 1997; Horrigan and Aldrich, 1999, 2002; Horrigan et al., 1999; Rothberg and Magleby, 1999, 2000; Cui and Aldrich, 2000). Functional BK channels are formed by homotetramers of α-subunits (Shen et al., 1994) each comprising a transmembrane voltage-sensing domain (VSD) and an intracellular Ca^{2+}-sensing C-terminal domain (CTD) that can independently modulate the ion conduction gate in the pore domain (PD) (Latorre et al., 2017). The CTDs consist of two non-identical regulators of the conductance of K^+ domains (RCK1 and RCK2) arranged into a ring-like tetrameric structure dubbed the gating ring (Wu et al., 2010; Yuan et al., 2010, 2012; Hite et al., 2017; Tao et al., 2017). Each RCK domain contains distinct ligand-binding sites capable of detecting Ca^{2+} in the micromolar range (Schreiber and Salkoff, 1997; Bao et al., 2002; Xia et al., 2002).

In the absence of Ca^{2+}, the activation of VSD decreases the free energy necessary to fully open the BK channels in an allosteric fashion (Horrigan and Aldrich, 1999; Horrigan et al., 1999). Under these experimental conditions, very positive membrane potentials are required to drive all voltage sensors to its activated conformation (Cui et al., 1997; Stefani et al., 1997; Horrigan et al., 1999; Contreras et al., 2012), ultimately leading to a significant activity of the BK channel. Hence, in cells like neurons, an appreciable open probability of

BK channels at physiologically relevant voltages necessarily involves the activation of Ca^{2+} sensors on the gating ring. The allosteric interplays established between the functional and structural modules (VSD-PD, CTD-PD, and CTD-VSD) are key in enabling BK channels to operate over a dynamic wide-range of internal Ca^{2+} and voltage conditions by fine-tuning the channel's gating machinery. Therefore, understanding the structure-functional bases that underlie the Ca^{2+} and voltage activation mechanisms interrelationship becomes essential.

The voltage dependence of Ca^{2+}-dependent gating ring rearrangements (Miranda et al., 2013, 2018) and RCK1 site occupancy (Sweet and Cox, 2008; Savalli et al., 2012; Miranda et al., 2018) as well as the perturbation of VSD movements by Ca^{2+} binding (Savalli et al., 2012) support the idea that the energetic interaction between both specialized sensors may be crucial to favor BK channel activation. The physical CTD-VSD interface has been suggested to provide the structure capable of mediating the crosstalk between these sensory modules and their synergy in activating the pore domain (Yang et al., 2007; Sun et al., 2013; Tao et al., 2017; Zhang et al., 2017). However, the strength of the interaction between voltage and Ca^{2+} sensors and their relevance to BK channel activation is still an unresolved matter (Horrigan and Aldrich, 2002; Carrasquel-Ursulaez et al., 2015). Also, the functional role that plays each of the high-affinity Ca^{2+}-binding sites on the CTD-VSD allosteric interaction is an open question. The RCK1 and RCK2 Ca^{2+}-binding sites have distinct functional properties conferred by their different molecular structures and relative positions within the gating ring (Wu et al., 2010; Yuan et al., 2010, 2012; Hite et al., 2017; Tao et al., 2017). Thus, the RCK sites differ in their Ca^{2+} binding affinities (Bao et al., 2002; Xia et al., 2002; Sweet and Cox, 2008), divalent cations selectivity (Oberhauser et al., 1988; Schreiber and Salkoff, 1997; Zeng et al., 2005; Zhou et al., 2012), voltage dependence (Sweet and Cox, 2008; Savalli et al., 2012; Miranda et al., 2018) and in their

64 contribution to allosteric gating mechanism (Yang et al., 2010, 2015). In particular, only
65 the RCK1 site appears to be involved in communicating the Ca^{2+}-dependent
66 conformational changes towards the membrane-spanning VSD (Savalli et al., 2012;
67 Miranda et al., 2018). Recently, the *Aplysia* BK structure shows that the N-lobe of RCK1
68 domain is in a non-covalent contact with the VSD and the S4-S5 linker being this RCK1-
69 VSD interaction surface rearranged when comparing the liganded and Ca^{2+}-free
70 structures (Hite et al., 2017; Tao et al., 2017). Actually, it has been hypothesized that any
71 Ca^{2+}-induced rearrangements of the gating ring should be ultimately transmitted to the
72 pore domain via the VSD (Hite et al., 2017; Zhou et al., 2017). Thus, defining what extent
73 Ca^{2+} binding influences to VSD is crucial in determining how important is the crosstalk
74 between sensors in decreasing the free energy necessary to open the BK channel.

75 Here, we examined the Ca^{2+}-dependence of the VSD activation estimating the allosteric
76 coupling between Ca^{2+} and voltage sensors. By analyzing gating currents under
77 unliganded and Ca^{2+}-saturated conditions, we found a strong energetic influence of the
78 Ca^{2+}-binding on the voltage sensors equilibrium in an independent manner of the channel
79 opening. These findings point out that a major component in the synergistic Ca^{2+} and
80 voltage activation of BK channels can reside on the sensory domains communication. We
81 also found that the Ca^{2+}-dependent behavior of the voltage sensor activation is consistent
82 with an CTD-VSD allosteric coupling that occurs through a concerted interaction scheme
83 where each Ca^{2+}-bound to high-affinity sites affect equally all voltage sensors in the BK
84 tetramer. Notably, we found that the two distinct RCK1 and RCK2 Ca^{2+} sensors exert
85 equivalent contributions on VSD via independent allosteric pathways.

Results

Allosteric coupling between Ca^{2+}-binding and voltage sensor activation is strong. We characterized the effects of Ca^{2+}-binding on voltage sensor activation in BK channels by analyzing gating current measured on inside-out patches of *Xenopus laevis* oocyte membrane. Families of gating currents (I_G) were evoked at different intracellular Ca^{2+} concentrations ($[Ca^{2+}]_i$) ranging from 0.1 to 100 µM in K^+-free solution (***Figure 1A***). For all experiments, first we measured I_G in the nominal absence of Ca^{2+} ("zero Ca^{2+}" condition), and then we perfused the internal side with solutions containing Ca^{2+} at increasing concentrations. The amount of gating charge displaced (Q_C) at each Ca^{2+} concentration was obtained by fitting the initial part of the ON-gating current decay to a single exponential (fast ON-gating; see *Methods*) and integrating it. In this manner, we determine only the gating charge displaced before the BK channel opening.

The increase in internal Ca^{2+} promotes a leftward shift of the Q_C versus voltage ($Q_C(V)$) curves (***Figure 1B,C***) which indicate that Ca^{2+}-binding facilitates the activation of the voltage sensor being more prominent as binding sites occupancy increases. Revealing a strong energetic interaction between both sensors, a significant Ca^{2+}-induced shift of voltage sensor activation occurs (ΔV_H = -142.6 ± 4.5 mV) under Ca^{2+}-saturated conditions for high-affinity binding sites (100 µM). Such large shift means that Ca^{2+}-binding to the RCK Ca^{2+}-binding sites alters the VSD equilibrium promoting a decrease in the free energy ($\Delta\Delta G_V^{Ca}$) that defines the voltage sensor resting-active (R-A) equilibrium by ~8 kJ/mol ($\Delta\Delta G_V^{Ca}$ = -7.98 ± 0.27 kJ/mol).

A visual inspection of the current records indicates that the kinetics of the ON-gating current is not much affected by the concentration of Ca^{2+} present in the internal solution.

However, it is apparent that the OFF-gating current is dramatically modified becoming smaller in amplitude and with slower kinetics as the internal Ca^{2+} concentration is increased (***Figure 1A*** and ***Figure 1—figure supplement 1A***). At least two components can be resolved in the OFF gating current decay (***Figure 1—figure supplement 1B,C***), and the relative contribution of the slower component increases as internal Ca^{2+} augmented reflecting an increase of the open probability of channel ***Figure 1—figure supplement 1D,E***). This kinetic behavior recapitulates the effect describe on gating charge displacement as a function of the depolarizing pulse duration (Horrigan and Aldrich, 2002; Contreras et al., 2012; Carrasquel-Ursulaez et al., 2015), and confirm that this phenomenon is associated with the time course of channel opening revealing the allosteric interaction between voltage sensors and the pore gate (Horrigan and Aldrich, 2002).

Ca^{2+} binding to single α-subunit affects the R-A voltage sensor equilibrium of all four subunits equally. Taking advantage of the dose-dependent effect of Ca^{2+} on voltage sensor activation we investigated the underlying mechanism of the Ca^{2+}-voltage sensors communication in the context of the well-established Horrigan-Aldrich (HA) allosteric gating model(Horrigan and Aldrich, 2002). Two different mechanisms were proposed by Horrigan and Aldrich for the interaction between the Ca^{2+}-binding sites and voltage sensors. The first mechanism supposes that Ca^{2+} binding to one α-subunit affects the VSD in the same subunit only (Scheme I) (***Figure 2A***), while the second mechanism assumes that the Ca^{2+} binding affects the four VSD equally (Scheme II) (***Figure 2B***). It should be noted that the standard HA model makes two simplifying assumptions by considering a

single Ca^{2+}-binding site per α-subunit and the Scheme I as the Ca^{2+} binding-VSD interaction mechanism underlying BK channel gating (Horrigan and Aldrich, 2002).

For a better comprehension, we simulated the normalized $Q_C(V)$ curves over a wide range of Ca^{2+} concentrations (from 0 to 10 mM) for each Ca^{2+}-VSD interaction scheme (***Figure 2C,D***). Here we assume that the measurement of the fast gating currents captures the charge displaced by R-A transitions and exclude the charge associated with the transition between the activated estates. This assumption is reasonable since the Ca^{2+}-binding rate constant estimated for BK is about 10^8 $M^{-1}s^{-1}$ (Hou et al., 2016) implying that at 10 µM internal Ca^{2+} (the highest non-saturating Ca^{2+} concentration tested) the time constant of the Ca^{2+} binding is 1 ms, while the VSD activates with a time constant of ~30 µs at the higher voltage tested (see the *Supplementary Information* for details of the simulations). At extreme conditions of low (0.03 to 0.1 µM) and high (≥100 µM) internal Ca^{2+}, the VSD activation behaves in a mechanism-independent manner since all voltage sensors are in the same functional state (unliganded or saturated). However, the distinctive effects on $Q_C(V)$ curves at intermediate Ca^{2+} concentrations (1-10 µM) provide useful signatures to distinguish between these two mechanisms. Scheme I predicts two functional states of the VSD depending on occupancy status of the Ca^{2+} site (Ca^{2+} bound and unbound) such that the $Q_C(V)$ curve behavior is described by the fractional distribution of the unliganded and Ca^{2+}-saturated functional states like an all-or-none allosteric effect (***Figure 2C***; ***Figure 2—figure supplement 1B*** and Equation 4 in *Supplementary Information*). On the contrary, the Ca^{2+}-binding effect on the VSD activation according to the Scheme II is characterized by a five-component Boltzmann function (***Figure 2—figure supplement 1C*** and Equation 6 in *Supplementary Information*). Each component represents a single functional state determined by the number of Ca^{2+} bound to the channel (from 0 to 4). In such case, the $Q_C(V)$ curves

resulting from a distribution of functional states behaves as an equivalent single Boltzmann leftward shifted by an incremental allosteric effect (from E to E^4) as the number of Ca^{2+} bound to the channel increases (***Figure 2D***).

To elucidate the mechanism by which Ca^{2+} and voltage sensors interact, we performed fits of the $Q_C(V)$ data using the two different models represented in the Scheme I and Scheme II (***Figure 3A,B***). The allosteric factor E that accounts for the coupling between the Ca^{2+}-binding sites and the voltage sensors was constrained to values calculated from the experimental data of the $Q_C(V)$ shift at the Ca^{2+} saturating conditions (100 µM) in relation to the same curve in the absence of Ca^{2+}. The z_J, J_0 and K_D parameters obtained during the fitting procedure of each model are very similar (***Figure 3C***). The fitted values of the affinity constant (K_D = 3 - 5 µM) agree with previous reports (Cox et al., 1997; Horrigan and Aldrich, 2002) although slightly smaller than those estimated on the closed conformation of the channel (K_D = 11 µM). However, we found that the fit with the Scheme II to the $Q_C(V)$ curves (***Figure 3B***) is better than the fit to the data using Scheme I (***Figure 3A***) as indicated by the Akaike model selection criteria (AIC) (Akaike, 1974). Moreover, Model II generates a V_H-$\log[Ca^{2+}]$ curve (solid line) that accounts for the dose-response V_H-$\log[Ca^{2+}]$ experimental data reasonable well (***Figure 3D***). Also, the behavior of $Q_C(V)$ curves at intermediate Ca^{2+} concentrations (1-10 µM) is qualitatively consistent with the phenotype exhibit by the Ca^{2+}-VSD scheme II (***Figure 2D*** **and** ***Figure 3B***). Thus, the experimental dose-dependent effect of Ca^{2+} on voltage sensor activation reveals that Ca^{2+}-binding to a single α-subunit of BK channels increases E-fold the equilibrium constant J that defines the equilibrium between resting and active conformations of the voltage sensors in all four subunits.

High-affinity Ca^{2+}-binding sites in RCK1 and RCK2 domains contribute equally to the allosteric coupling between Ca^{2+} and voltage sensors. Under physiological conditions, the RCK1 and RCK2 high-affinity Ca^{2+}-binding sites are responsible by all calcium sensitivity of the activation of BK channel (Schreiber and Salkoff, 1997; Bao et al., 2002, 2004; Xia et al., 2002). However, distinct physiological roles of the RCK1 Ca^{2+}-sensor and Ca^{2+} bowl may be based in their functionally and structurally distinctive properties (Zeng et al., 2005; Sweet and Cox, 2008; Yang et al., 2010; Savalli et al., 2012; Tao et al., 2017). Below, we asked what the energetic contribution to VSD equilibrium is of the two high-affinity Ca^{2+}-binding sites contained in the RCK1 and RCK2 domains.

To elucidate the effect of each Ca^{2+}-sensor on the VSD activation we used mutations that selectively and separately abolish the function of the two differents RCK Ca^{2+}-sites. Disruption of the RCK1 Ca^{2+}-sensor by the double mutant D362A/D367A (Xia et al., 2002) reduces significantly (48%, $\Delta V_{H\ (D362A/D367A)}$ = -74.9 ± 4.7 mV) the leftward shifted of the $Q_C(V)$ curves at 100 µM Ca^{2+} compared with the wild-type (WT) BK channel (***Figure 4A,C***). We also examined the effect of the mutant M513I (Bao et al., 2002) which have been shown to eliminate the Ca^{2+} sensitivity derived from the RCK1 site (Bao et al., 2002, 2004; Zhang et al., 2010). In this mutant, the 100 µM Ca^{2+}-induced shift in V_H of VSD activation curve is also considerably smaller relative to WT (about 54%, $\Delta V_{H\ (M513I)}$ = -65.4 ± 2.6 mV) (***Figure 5***). Therefore, both mutations affect the Ca^{2+}-induced enhancement of activation of voltage sensor very similarly through the RCK1 site (***Figure 5C***), although their mechanisms action could be quite different. The M513 residue appears to participate in the stabilization of the proper conformation RCK1 Ca^{2+}-site whereas D367 is a key residue in the coordination of Ca^{2+} ion (Wu et al., 2010; Zhang et al., 2010; Tao et al., 2017). On the other hand, neutralization of the residues forming part of the Ca^{2+} bowl (Schreiber and Salkoff, 1997) (5D5A mutant, see *Methods*) on the RCK2 domain

decreases the leftward shift of the $Q_C(V)$ curve when Ca^{2+} is increased to 100 μM by approximately 54% ($\Delta V_{H\ (5D5A)}$ = -65.7 ± 4.7 mV) (***Figure 4B, D***). Surprisingly, the effect of Ca^{2+} binding on ΔV_H from each high-affinity Ca^{2+} site is roughly half relative to WT channels with both intact sites (***Figure 4E***). Therefore, both high-affinity Ca^{2+}-binding sites contribute equally to decrease the free energy necessary to activate the VSD. Thus, the change of free energy of the resting-active equilibrium of the voltage sensor in response to Ca^{2+}-binding at RCK2 site is ~ -4 kJ/mol ($\Delta\Delta G_V^{Ca}{}_{(D362A/D367A)}$ = -4.2 ± 0.3 kJ/mol and $\Delta\Delta G_V^{Ca}{}_{(M513I)}$ = -3.6 ± 0.5 kJ/mol) (***Figure 4C*** and ***Figure 5C***). In the same way, the occupation of the RCK1 Ca^{2+}-binding site decreases the free energy necessary to activate the VSD in -3.8 ± 0.4 kJ/mol ($\Delta\Delta G_V^{Ca}{}_{(5D5A)}$). Remarkably, these findings reveal an additive effect of Ca^{2+}-binding to the RCK1 and Ca^{2+} bowl sites on the VSD activation which suggest independent allosteric pathways through which they exert their modulation on the VSD.

Taking these results into account, we expanded the Ca^{2+}-VSD interaction model described by Scheme II considering the energetic contribution of the two kinds of Ca^{2+} sensors on the VSD per α-subunit ($E_{WT} = E_{S1} * E_{S2}$) (***Figure 2—figure supplement 1E***). As described in the above model fittings, the allosteric factors E of each one RCK1 and RCK2 sites (E_{S1} and E_{S2}) were constrained to values equivalent to the Ca^{2+}-induced energetic perturbations of the voltage sensor equilibrium for the 5D5A and D362A/D367A mutants, respectively. However, the inclussion of the two Ca^{2+} sensors in the Ca^{2+}-VSD interaction model does not produce better fits to $Q_C(V, [Ca^{2+}])$ according to the AIC criteria (***Table 1*** and ***Figure 3B***), the estimated K_D parameters for each Ca^{2+}-binding sites (K_{D1} = 15.6 μM and K_{D2} = 1.9 μM) by the experimental data fitting agrees very well with the apparent

227 Ca^{2+} affinities previously reported in the literature (Bao et al., 2002; Xia et al., 2002; Sweet
228 and Cox, 2008). Interestingly, modest positive cooperativity (G = 2.6) between the two
229 Ca^{2+}-binding sites located in the same α-subunit is required to achieve a good estimation
230 of the K_D parameters (***Table 1***), where the Ca^{2+} bowl site has an affinity for Ca^{2+} about 8-
231 fold greater than does the RCK1 Ca^{2+}-sensor.

Discussion

Recent insights into a major interplay between voltage- and Ca^{2+}-sensing modules in the BK channel are supported by functional and structural studies (Yuan et al., 2010; Savalli et al., 2012; Miranda et al., 2013, 2016, 2018; Carrasquel-Ursulaez et al., 2015; Hite et al., 2017; Tao et al., 2017; Zhang et al., 2017), offering a new perspective in our understanding of its multimodal gating mechanism. However, the CTD-VSD allosteric coupling as well its molecular nature has yet to be firmly established since their direct assessment is subject to great experimental challenges. Based on the functional independence of the distinct structural domains (PD, CTD, and VSD), the energetic relationship between the sensory modules can be directly defined comparing the voltage sensor equilibrium change at extreme Ca^{2+} stimulus conditions limiting the status of the Ca^{2+}-binding sites to two well-defined configurations: unliganded and saturated (Horrigan and Aldrich, 2002).

Using this approach, this work straightforwardly establishes that Ca^{2+}-binding to high-affinity sites make a significant and direct energetic contribution to the equilibrium of the resting-activated transition (R-A) of the VSD facilitating their activation (ΔV_{H} = -142.6 ± 4.5 mV and $\Delta\Delta G_V^{Ca}$ = -7.98 ± 0.27 kJ/mol). This result resolves a previous debate regarding to the magnitude of the Ca^{2+}-driven shift of the $Q_{\mathrm{C}}(V)$ curve, because it has been reported a similar leftward shift (ΔV_{H} = -140 mV and $\Delta\Delta G_V^{Ca}$ = -7.9 kJ/mol; at $[Ca^{2+}]_i$ = 100 µM) (Carrasquel-Ursulaez et al., 2015) and a smaller leftward shift (ΔV_{H} = -33 mV and $\Delta\Delta G_V^{Ca}$ = -1.9 kJ/mol; at $[Ca^{2+}]_i$ = 70 µM) (Horrigan and Aldrich, 2002) at saturating Ca^{2+} concentration. The reason for the contradictory findings is not clear to us; since we used a similar experimental approach. Even if we assumed that the calcium effect on VSD is underestimated at 70 µM Ca^{2+} (Horrigan and Aldrich, 2002) compared to 100 µM as

saturating condition of the binding sites, we observed a significative greater effect in Ca^{2+} concentrations (1, 5 and 10 µM, ***Figure 1C***) where less than 50% of the Ca^{2+} sensors are occupied (K_D = 11 µM (Cox et al., 1997; Horrigan and Aldrich, 2002)).

Fluorescence studies that optically track the motions of the voltage sensor or gating ring provide two lines of evidence that support these findings. First, conformational rearrangements of the voltage sensors detected using voltage-clamp fluorometry can be provoked by Ca^{2+}-binding to the high-affinity sites. The sudden rise of intracellular [Ca^{2+}] by UV flash induced-photolysis of caged Ca^{2+} prompts a leftward shift in both conductance-voltage ($G(V)$) and fluorescence-voltage ($F(V)$) relationships. These results suggest that functional activation of the gating ring is propagated to VSD leading to structural perturbations of voltages sensors, thereby favoring its active conformation (Savalli et al., 2012). Second, the structural rearrangement of gating ring in response to Ca^{2+} has a voltage dependence (Miranda et al., 2013, 2018) attributable to the voltage sensor operation. The origin of these voltage-dependent motions has been recently established via modifications on the voltage-sensing function of the BK channel using the patch-clamp fluorometry technique (Miranda et al., 2018). Both the charged residue mutations on the S4 transmembrane segment (R210, R213, and E219) and the co-expression of β1-subunit with BKα channel modify the conformational changes of the gating ring triggered by depolarization in correspondence to the observed $G(V)$ shift for these channel constructs. In contrast, perturbations of pore opening equilibrium like the F315A mutation or the assembly of BKα channel with γ1-subunit does not modify on the voltage-dependent reorganization of the gating ring (Miranda et al., 2018).

Mechanistically and in a channel opening-independent fashion, how does the CTD-VSD coupling occur? Taking into account the homotetrameric configuration of the BK channel, Horrigan and Aldrich (Horrigan and Aldrich, 2002) defined the general gating scheme of

BK channel considering the simplest CTD-VSD interaction model in which voltage sensors and Ca^{2+}-binding sites solely interact within the same subunit. However, the VSD movement at non-saturating Ca^{2+} conditions which entail distinct functional states of the Ca^{2+} sites (unliganded and liganded), unveiled that the standard HA model can not explain the mechanistic interaction governing the allosteric coupling between the Ca^{2+} and voltage sensors. Given that Ca^{2+}-binding will influence only a fraction of voltage sensors, Scheme I would evidence $Q_C(V)$ curves characteristic of an all-or-none model showing two well-distinguishable components Boltzmann that correspond to Ca^{2+}-affected and unaffected VSD fractions (***Figure 3A***). Conversely, an energetic effect of each Ca^{2+}-site on all the voltage sensors of the tetramer would lead to an equivalent functional status of each VSD, so that the $Q_C(V)$ curves behaving in an incremental shifted fashion as increasing the fractional occupancy of the Ca^{2+} sites. The VSD and Ca^{2+} sites interacting in such a fashion (Scheme II) reproduce reasonably well the behavior of the Ca^{2+}-dependent gating charge movement observed in our experiments (***Figure 3B***). This concerted CTD-VSD communication may underlie a mechanism analogous to the mechanical strategy of interaction between the homooctameric ring of RCK domains and the pore module described for bacterial K^+ channels (Jiang et al., 2002; Ye et al., 2006; Lingle, 2007; Pau et al., 2011; Smith et al., 2012, 2013). Both in MthK and BK channels, the Ca^{2+}-site occupancy triggers a conformational change conveying to a symmetric overall rearrangement of the cytosolic tetrameric structure that finally is propagated to the transmembrane regions (TMD) via C-linker and in the BK channel also via the protein-protein interfaces between the gating ring and the TMD (Jiang et al., 2002, 2003; Ye et al., 2006; Yuan et al., 2010, 2012; Pau et al., 2011; Smith et al., 2012; Tao et al., 2017). Consequently, we can speculate that each Ca^{2+}-binding event produces a gradual

conformational expansion of the gating ring affecting the four voltage sensors in each step through the progressive perturbations within the protein-protein interfaces.

As mentioned above, the communication pathway through which the Ca^{2+}-driven conformational changes are propagated to the voltage sensors appears to critically reside on the CTD-VSD interface that involves non-covalent interactions between RCK1 N-lobe and S0-S4 transmembrane segments (Yang et al., 2007, 2008, 2010; Sun et al., 2013; Hite et al., 2017; Tao et al., 2017). Scanning mutagenesis of RCK1-N terminal subdomain indicated that residues on the βA-αC region are involved into the allosteric connection of the Ca^{2+}-dependent activation mediated by RCK1 site occupancy but not to the Ca^{2+} bowl (Yang et al., 2010). In line with this study, the selective activation of the RCK1 domain was identified to be responsible for the Ca^{2+}-induced VSD rearrangement (Savalli et al., 2012) and the voltage dependence of the Ca^{2+}-driven motions of gating ring (Miranda et al., 2016, 2018), suggesting that CTD-VSD allosteric coupling is primarily determined by the RCK1 site. However, our results are inconsistent with this picture. The constructs D362A/D367A and 5D5A (D894A-D898A) selectively impaired the Ca^{2+}-sensitivity of the RCK1- and RCK2-sensors, respectively, by neutralization of residues that are involved in contributing to Ca^{2+}-coordination (Zhang et al., 2010; Tao et al., 2017). Comparing the fast gating charge movement at 0 Ca^{2+} and saturating Ca^{2+} conditions reflects that the energetic effect of Ca^{2+}-binding on voltage sensor equilibrium is practically identical (~ -4 kJ/mol) for either the D362A/D367A mutations or 5D5A mutations (***Figure 4***). Thus, our findings establish that the RCK2-driven contribution to CTD-VSD energetic coupling is quite similar to the RCK1-driven contribution. The functional role of the RCK2-sensor on Ca^{2+}-sensitivity of VSD activation was further corroborated using the M513I mutation (***Figure 5***). This point mutation hinders the Ca^{2+}-dependent activation associated with the RCK1-sensor presumably by disrupting the structural integrity of the binding site and the

transduction via through the βA-αC region (Zhang et al., 2010). Thus, another residue involved in the BK Ca^{2+}-dependent activation mediated by the RCK1 Ca^{2+}-binding site but not forming part of the site itself decreases the $Q_C(V)$ leftward shift almost in the same amount as it does the D362A/D367A mutant.

Interestingly, beyond the energetic contribution of each RCK site to the voltage sensor equilibrium is the same, its addition mimics the VSD Ca^{2+}-sensitivity of the fully occupied sites. These findings remind us of early reports showing that each RCK site mutant shifts the Ca^{2+}-dependent $G(V)$ by approximately half relative to WT channels (Bao et al., 2002; Xia et al., 2002). Our results suggest an autonomy of the two RCK-sensors indicating independent allosteric pathways through which they exert their modulation on the VSD but does not discard some cooperativity effect between them. Indeed, various lines of evidence indicate albeit modest a cooperativity between the two high-affinity Ca^{2+}-binding sites although their nature is still unclear (Qian et al., 2006; Sweet and Cox, 2008; Savalli et al., 2012). Intra and intersubunit structural connectivity support the putative cooperative interactions between the Ca^{2+} sensors at the gating ring (Yuan et al., 2012; Hite et al., 2017). Actually, a recently functional study of the intrasubunit connections between the RCK1 site and Ca^{2+} bowl (R514-Y904/E902 interactions) has shown that such connections are potential candidates of the structural determinants underlying to a cooperative mechanism between the RCK1- and RCK2-sensor involving either to preserve the integrity of RCK1 Ca^{2+}-binding site or the allosteric propagation pathway towards transmembrane domains (Kshatri et al., 2018). On the basis of the cryo-EM structure of *Aplysia californica* BK channel, Hite *et al*. (Hite et al., 2017) proposed that there should be a positive cooperativity of the Ca^{2+}-binding at RCK1 site and Ca^{2+} bowl since the Ca^{2+}-induced conformational change of the RCK1-N lobes from closed to open configuration depends on functional state (unliganded and liganded) of both RCK sites.

Our analysis based on the CTD-VSD interaction model predicted a small and positive cooperative relation (G = 2.6) among the two high-affinity Ca^{2+} sites within the same α-subunit, which has been suggested by an earlier study (Qian et al., 2006). It is noteworthy that K_D parameters achieved for each Ca^{2+}-binding sites (K_{D1} = 15.6 μM and K_{D2} = 1.9 μM) by the experimental data fitting agrees very well with the apparent Ca^{2+} affinities previously reported in the literature (Bao et al., 2002; Xia et al., 2002; Sweet and Cox, 2008). Together, all this new information recapitulate a more relevant functional role of the cooperative interactions between RCK sensors within the same subunit on Ca^{2+}-dependent activation of the channel (Qian et al., 2006).

In conclusion, our results depict a remarkable, and direct energetic direct interplay between the specialized sensory modules (VSD and CTD). Our findings together with the emerging structural-functional information establish a new paradigm about how the stimuli integration (depolarization and intracellular Ca^{2+}) modulates the BK channel activation and its relevance within a physiological context. Notable and unexpected is the equivalent role of the distinct ligand-binding sites at the cytosolic domain to the allosteric regulation on voltage sensing. Additional studies to discern the molecular bases underlying in the Ca^{2+} and voltage propagation pathways and the cooperative interactions of the RCK1 and RCK2 regulatory domains may provide new clues about the dual gating mechanism of BK channel.

Methods

Channel Expression.

Xenopus laevis oocytes were used as a heterologous system to express BK channels. The cDNA coding for the human BK α-subunit (U11058) was provided by L. Toro (University of California, Los Angeles, CA). The cDNA coding for independent mutants of each two high-affinity Ca^{2+} site from BK channel, the double mutant D362A/D367A (Xia et al., 2002) and the mutant M513I (Bao et al., 2002) in the RCK1 Ca^{2+}-binding site and the mutant 5D5A (Schreiber and Salkoff, 1997) (D894A/D895A/D896A/D897A/D898A) in the RCK2 Ca^{2+}-binding site or calcium bowl, were kindly provided by M. Holmgren (National Institutes of Health, Bethesda, MD). The cRNA was prepared by using mMESSAGE mMACHINE (Ambion) for *in vitro* transcription. *Xenopus laevis* oocytes were injected with 50 ng of cRNA and incubated in an ND96 solution (in mM: 96 NaCl, 2 KCl, 1.8 $CaCl_2$, 1 $MgCl_2$, 5 HEPES, pH 7.4) at 18°C for 4–8 days before electrophysiological recordings.

Electrophysiological recordings.

All recordings were made by using the patch-clamp technique in the inside-out configuration. Data were acquired with an Axopatch 200B (Molecular Devices) amplifier and the Clampex 10 (Molecular Devices) acquisition software. Gating current (I_G) records were elicited by 1-ms voltage steps from −90 to 350 mV in increments of 10 mV. Both the voltage command and current output were filtered at 20 kHz with 8-pole Bessel low-pass filter (Frequency Devices). Current signals were sampled with a 16-bit A/D converter (Digidata 1550B; Molecular Devices), using a sampling rate of 500 kHz. Linear membrane capacitance and leak subtraction were performed based on a P/4 protocol (Armstrong and Bezanilla, 1974).

Borosilicate capillary glasses (1B150F-4, World Precision Instruments) were pulled in a horizontal pipette puller (Sutter Instruments). After fire-polished, pipette resistance was 0.5-1 MΩ. The external (pipette) solution contained (in mM): 110 tetraethylammonium (TEA)-$MeSO_3$, 10 HEPES, 2 $MgCl_2$; pH was adjusted to 7.0. The internal solution (bath) contained (in mM): N-methyl-D-glucamine (NMDG)-$MeSO_3$, 10 HEPES, and 5 EGTA for "zero Ca^{2+}" solution (~0.8 nM, based on the presence of ~10 μM contaminant $[Ca^{2+}]$ (Cui et al., 1997). For test solutions at different Ca^{2+} concentrations (0.1-100 μM), $CaCl_2$ was added to reach the desired free $[Ca^{2+}]$, and 5 mM EGTA (0.1-0.5 μM) or HEDTA (1-10 μM) was used as calcium buffer. No Ca^{2+} chelator was used in 100 μM free Ca^{2+} solutions. Free calcium concentration was estimated using the WinMaxChelator Software and checked with a Ca^{2+}-electrode (Hanna Instruments). All experiments were performed at room temperature (20-22 °C). To measure I_G at different Ca^{2+} concentrations in the same oocyte, the patch was excised and washed with an appropriate internal solution at least 10 times the chamber volume.

Data Analysis.

All data analysis was performed using Clampfit 10 (Molecular Devices), Matlab (MathWorks) and Excel 2007 (Microsoft). The first 50-100 μs of the ON-gating currents were fitted to a single exponential function and the area under the curve was integrated to obtain the charge displaced between closed states (Q_C) (Horrigan and Aldrich, 1999, 2002; Contreras et al., 2012; Carrasquel-Ursulaez et al., 2015). $Q_C(V)$ data for each $[Ca^{2+}]_i$ were fitted using a Boltzmann function: $Q_C(V) = \frac{Q_{C,\ MAX}}{1+e^{\left(\frac{-z_Q F(V-V_H)}{RT}\right)}}$, where $Q_{C,\ MAX}$ is the maximum charge, z_Q is the voltage dependency of activation, V_H is the half-activation voltage, T is the absolute temperature (typically 295 K), F is the Faraday's

constant, and R is the universal gas constant. $Q_{\mathrm{C,\ MAX}}$, V_{H}, and z_Q were determined using least square minimization. $Q_{\mathrm{C}}(V)$ curves were aligned by shifting them along the voltage axis by the mean $\Delta V = (\langle V_{\mathrm{H}} \rangle - V_{\mathrm{H}})$ to generate a mean curve that did not alter the voltage dependence (Horrigan and Aldrich, 1999). All error estimates are SEM.

The Ca^{2+}-induced effect on VSD activation was quantified as the V_{H} shift relative to "zero" Ca^{2+} condition: $\Delta V_{\mathrm{H}} = V_{\mathrm{H}\left([\mathrm{Ca}^{2+}]_i\right)} - V_{\mathrm{H}\left(0\,[\mathrm{Ca}^{2+}]_i\right)}$. For wild-type (WT) BK channel and the RCK Ca^{2+}-sensor mutants (D362A/D367A, M513I and 5D5A), the energetic contribution of Ca^{2+}-binding on resting-active (R-A) equilibrium of the voltage sensor was calculated as changes in Gibbs free energy of VSD activation induced by 100 µM Ca^{2+}:

$$\Delta\Delta G_V^{Ca} = F\left(z_{Q\left(100\ \mu\mathrm{M}\,[\mathrm{Ca}^{2+}]_i\right)} V_{\mathrm{H}\left(100\ \mu\mathrm{M}\,[\mathrm{Ca}^{2+}]_i\right)} - z_{Q\left(0\,[\mathrm{Ca}^{2+}]_i\right)} V_{\mathrm{H}\left(0\,[\mathrm{Ca}^{2+}]_i\right)}\right).$$

Model fitting.

We fit the $Q_{\mathrm{C}}(V, [\mathrm{Ca}^{2+}])$ experimental data using two distinct interaction mechanism between Ca^{2+}-binding sites and voltage sensor (see Scheme I and Scheme II in the ***Figure 2A,B***) within the framework of Horrigan-Aldrich (HA) general allosteric model (Horrigan and Aldrich, 2002). Assumptions and considerations for the equations that describe each one of the Ca^{2+}-VSD interaction schemes are given in the *Supplementary Information*. In terms of the HA allosteric mechanisms, the voltage sensor R-A equilibrium is defined by the equilibrium constant J according to the relation $J = e^{\frac{z_J F(V - V_{\mathrm{H}})}{RT}} = J_0 e^{\frac{z_J F V}{RT}}$, where J_0 is the zero voltage equilibrium constant and z_J the gating charges displacement per voltage sensor. In this fashion, the fraction of the total charge displaced essentially between closed states, $\left(Q_{\mathrm{C}}(V)/Q_{\mathrm{C,\ MAX}}\right)$ in the absence of calcium can be written as:

$Q_{\mathrm{C}}(V)/Q_{\mathrm{C,\ MAX}}\ (\mathrm{Ca}^{2+} \ll K_D) = \frac{1}{1+J^{-1}}$, where K_D is the dissociation constant of the high-affinity calcium-binding site with all voltage sensors at rest and the channel closed. In the presence of saturating Ca^{2+} (100 µM), the equilibrium of the R-A transition J becomes amplified by the allosteric factor E, which defines the coupling between Ca^{2+}-binding sites and voltage sensors, being $Q_{\mathrm{C}}(V)/Q_{\mathrm{C,\ MAX}}\ (\mathrm{Ca}^{2+} \gg K_D) = \frac{1}{1+(JE)^{-1}}$ and $JE = J_0 e^{\frac{RT\ln(E)+z_J FV}{RT}}$. The $Q_{\mathrm{C}}(V)/Q_{\mathrm{C,\ MAX}}$ measured in the presence of high $[Ca^{2+}]$ and "zero Ca^{2+}" condition at the same voltage (so that J be canceled out) but in the limit where voltage where $J^{-1} \gg 1$ is :

$$\frac{Q_{\mathrm{C}}(V)/Q_{\mathrm{C,\ MAX}}\ (\mathrm{Ca}^{2+} \gg K_D)}{Q_{\mathrm{C}}(V)/Q_{\mathrm{C,\ MAX}}\ (\mathrm{Ca}^{2+} \ll K_D)}_{(\lim J^{-1} \gg 1)} = \frac{JE}{J} = E$$

Thus, the Gibbs free energy perturbation of the voltage sensor R-A equilibrium when the high-affinity binding sites are approximately 100% occupied by Ca^{2+} (100 µM) is a straightforward measure of the allosteric factor E: $E = e^{-\Delta\Delta G_V^{Ca}/RT}$.

Based on these conditions, the allosteric parameter E values were calculated and introduced in each of the two Ca^{2+}-VSD interaction models as a fixed parameter. Once E was obtained, the families of $Q_{\mathrm{C}}(V, [\mathrm{Ca}^{2+}])$ curves were simultaneously fitted to the model equations (Equation 3 and Equation 6) (see *Supplementary information*) by minimizing least-squares estimating the z_J, J_0 and K_D parameters for each model. To select the better Ca^{2+}-VSD interaction scheme that describes the experimental data, the model fits were compared according to their Akaike Information Criterion (AIC) (Akaike, 1974) values, calculated as $\mathrm{AIC} = 2p - 2\ln(L)$, where p is the number of free

parameters and $\ln(L)$ is the maximum log-likelihood of the model. The best model fitting is that achieving the lowest AIC values. Minimum AIC values were used as model selection criteria.

The best model fit of the Ca^{2+}-VSD interaction scheme was extended including two high-affinity Ca^{2+}-binding sites per α-subunit (***Figure 2—figure supplement 2D,E***). The contribution of each Ca^{2+}-binding site to the free energy of the voltage sensor equilibrium may be split in two, such as $E = E_{S1} * E_{S2} = e^{-\left(\Delta\Delta G_V^{Ca}(S1) + \Delta\Delta G_V^{Ca}(S2)\right)/RT}$, where E_{S1} and E_{S2} are the allosteric factor E for the RCK1 and RCK2 sites. Thus, for the global fit of the $Q_C(V, [Ca^{2+}])$ curves, we constrained the allosteric parameter E_{S1} and E_{S2} obtained experimentally for the RCK2 Ca^{2+}-sensor mutant (5D5A) and RCK1 Ca^{2+}-sensor mutant (D362A/D367A), respectively, as described above. The rest of the parameters z_J, J_0, K_{D1}, K_{D2}, and G, where K_{D1} and K_{D2} are the dissociation constants of the RCK1 and RCK2 sites and G is a cooperativity factor between the two sites within the same α-subunit of the BK channel, were allowed to vary freely.

References

Akaike H. 1974. A new look at the statistical model identification. *IEEE Trans Automat Contr* **19**:716–723. DOI:10.1109/TAC.1974.1100705

Armstrong CM, Bezanilla F. 1974. Charge movement associated with the opening and closing of the activation gates of the Na channels. *J Gen Physiol* **63**:533–552. DOI:10.1085/jgp.63.5.533

Bao L, Rapin AM, Holmstrand EC, Cox DH. 2002. Elimination of the BKCa Channel's High-Affinity Ca2+ Sensitivity. *J Gen Physiol* **120**:173–189. DOI:10.1085/jgp.20028627

Bao L, Kaldany C, Holmstrand EC, Cox DH. 2004. Mapping the BK Ca Channel's "Ca2+ Bowl." *J Gen Physiol* **123**:475–489. DOI:10.1085/jgp.200409052

Carrasquel-Ursulaez W, Contreras GF, Sepúlveda R V, Aguayo D, González-Nilo F, González C, Latorre R. 2015. Hydrophobic interaction between contiguous residues in the S6 transmembrane segment acts as a stimuli integration node in the BK channel. *J Gen Physiol* **145**:61–74. DOI:10.1085/jgp.201411194

Contreras GF, Neely A, Alvarez O, Gonzalez C, Latorre R. 2012. Modulation of BK channel voltage gating by different auxiliary β subunits. *Proc Natl Acad Sci USA* **109**:18991–6. DOI:10.1073/pnas.1216953109

Cox DH, Cui J, Aldrich RW. 1997. Allosteric gating of a large conductance Ca-activated K+ channel. *J Gen Physiol* **110**:257–281. DOI:10.1085/jgp.110.3.257

Cui J, Cox DH, Aldrich RW. 1997. Intrinsic voltage dependence and Ca2+ regulation of mslo large conductance Ca-activated K+ channels. *J Gen Physiol* **109**:647–673. DOI:10.1085/jgp.109.5.647

Cui J, Aldrich RW. 2000. Allosteric Linkage between Voltage and Ca2+-Dependent Activation of BK-Type mslo1 K+ Channels. *Biochemistry* **39**:15612–15619. DOI:10.1021/bi001509+

501 Hite RK, Tao X, MacKinnon R. 2017. Structural basis for gating the high-conductance
502 Ca2+-activated K+ channel. *Nature* **541**:52–57. DOI:10.1038/nature20775
503 Horrigan FT, Cui J, Aldrich RW. 1999. Allosteric voltage gating of potassium channels I.
504 Mslo ionic currents in the absence of Ca2+. *J Gen Physiol* **114**:277–304.
505 Horrigan FT, Aldrich RW. 1999. Allosteric voltage gating of potassium channels II. Mslo
506 channel gating charge movement in the absence of Ca2+. *J Gen Physiol* **114**:305–
507 336. DOI:10.1085/jgp.114.2.305
508 Horrigan FT, Aldrich RW. 2002. Coupling between voltage sensor activation, Ca2+ binding
509 and channel opening in large conductance (BK) potassium channels. *J Gen Physiol*
510 **120**:267–305. DOI:10.1085/jgp.20028605
511 Hou P, Xiao F, Liu H, Yuchi M, Zhang G, Wu Y, Wang W, Zeng W, Ding M, Cui J, Wu Z,
512 Wang L-Y, Ding J. 2016. Extrapolating microdomain Ca2+ dynamics using BK
513 channels as a Ca2+ sensor. *Sci Rep* **6**:17343. DOI:10.1038/srep17343
514 Jiang Y, Lee A, Chen J, Cadene M, Chait BT, Mackinnon R. 2002. Crystal structure and
515 mechanism of a calcium-gated potassium channel 515–522.
516 Jiang Y, Ruta V, Chen J, Lee A, Mackinnon R. 2003. The principle of gating charge
517 movement in a voltage-dependent K channel. *Nature* **423**:42–48.
518 Kshatri AS, Gonzalez-Hernandez AJ, Giraldez T. 2018. Functional validation of Ca2+-
519 binding residues from the crystal structure of the BK ion channel. *BBA - Biomembr*
520 **1860**:943–952. DOI:10.1016/j.bbamem.2017.09.023
521 Latorre R, Castillo K, Carrasquel-Ursulaez W, Sepulveda R V, Gonzalez-Nilo F, Gonzalez
522 C, Alvarez O. 2017. Molecular Determinants of BK Channel Functional Diversity and
523 Functioning. *Physiol Rev* **97**:39–87. DOI:10.1152/physrev.00001.2016
524 Latorre R, Vergara C, Hidalgo C. 1982. Reconstitution in planar lipid bilayers of a Ca2+-
525 dependent K+ channel from transverse tubule membranes isolated from rabbit
526 skeletal muscle. *Proc Natl Acad Sci USA* **79**:805–809. DOI:10.1073/pnas.79.3.805

527 Lingle CJ. 2007. Gating Rings Formed by RCK Domains: Keys to Gate Opening. *J Gen*
528 *Physiol* **129**:101–107. DOI:10.1085/jgp.200709739
529 Marty A. 1981. Ca-dependent K channels with large unitary conductance in chromaffin
530 cell membranes. *Nature* **291**:497–500.
531 Miranda P, Contreras JE, Plested AJR, Sigworth FJ, Holmgren M, Giraldez T. 2013. State-
532 dependent FRET reports calcium- and voltage-dependent gating-ring motions in BK
533 channels. *Proc Natl Acad Sci USA* **110**:5217–5222. DOI:10.1073/pnas.1219611110
534 Miranda P, Holmgren M, Giraldez T. 2018. Voltage-dependent dynamics of the BK
535 channel cytosolic gating ring are coupled to the membrane-embedded voltage
536 sensor. *Elife* **7**:e40664. DOI:10.7554/eLife.40664
537 Miranda P, Giraldez T, Holmgren M. 2016. Interactions of divalent cations with calcium
538 binding sites of BK channels reveal independent motions within the gating ring. *Proc*
539 *Natl Acad Sci USA* **113**:14055–14060. DOI:10.1073/pnas.1611415113
540 Oberhauser A, Alvarez O, Latorre R. 1988. Activation by divalent cations of a Ca2+-
541 activated K+ channel from skeletal muscle membrane. *J Gen Physiol* **92**:67–86.
542 DOI:10.1085/jgp.92.1.67
543 Pallotta BS, Magleby KL, Barrett JN. 1981. Single channel recordings of Ca2+-activated
544 K+ currents in rat muscle cell culture. *Nature* **293**:471–474.
545 Pau VPT, Smith FJ, Taylor AB, Parfenova L V, Samakai E, Callaghan MM, Abarca-
546 Heidemann K, Hart PJ, Rothberg BS. 2011. Structure and function of multiple Ca2+-
547 binding sites in a K+ channel regulator of K+ conductance (RCK) domain. *Proc Natl*
548 *Acad Sci USA* **108**:17684–17689. DOI:10.1073/pnas.1107229108
549 Qian X, Niu X, Magleby KL. 2006. Intra- and Intersubunit Cooperativity in Activation of BK
550 Channels by Ca2+. *J Gen Physiol* **128**:389–404. DOI:10.1085/jgp.200609486
551 Rothberg BS, Magleby KL. 1999. Gating kinetics of single large-conductance Ca2+-
552 activated K+ channels in high Ca2+ suggest a two-tiered allosteric gating

mechanism. *J Gen Physiol* **114**:93–124. DOI:10.1085/jgp.114.1.93

Rothberg BS, Magleby KL. 2000. Voltage and Ca2+ activation of single large-conductance Ca2+-activated K+ channels described by a two-tiered allosteric gating mechanism. *J Gen Physiol* **116**:75–99. DOI:10.1085/jgp.116.1.75

Savalli N, Pantazis A, Yusifov T, Sigg D, Olcese R. 2012. The contribution of RCK domains to human BK channel allosteric activation. *J Biol Chem* **287**:21741–21750. DOI:10.1074/jbc.M112.346171

Schreiber M, Salkoff L. 1997. A novel calcium-sensing domain in the BK channel. *Biophys J* **73**:1355–1363. DOI:10.1016/S0006-3495(97)78168-2

Shen KZ, Lagrutta A, Davies NW, Standen NB, Adelman JP, North RA. 1994. Tetraethylammonium block of Slowpoke calcium-activated potassium channels expressed in Xenopus oocytes: evidence for tetrameric channel formation. *Pflugers Arch* **426**:440–445.

Smith FJ, Pau VPT, Cingolani G, Rothberg BS. 2012. Crystal structure of a Ba2+-bound gating ring reveals elementary steps in RCK domain activation. *Structure* **20**:2038–2047. DOI:10.1016/j.str.2012.09.014

Smith FJ, Pau VPT, Cingolani G, Rothberg BS. 2013. Structural basis of allosteric interactions among Ca2+-binding sites in a K+channel RCK domain. *Nat Commun* **4**:1–10. DOI:10.1038/ncomms3621

Stefani E, Ottolia M, Noceti F, Olcese R, Wallner M, Latorre R. 1997. Voltage-controlled gating in a large conductance Ca2+ sensitive K+ channel (hslo). *Proc Natl Acad Sci USA* **94**:5427–5431.

Sun X, Shi J, Delaloye K, Yang X, Yang H, Zhang G, Cui J. 2013. The Interface between Membrane-Spanning and Cytosolic Domains in Ca2+-Dependent K+ Channels Is Involved in Subunit Modulation of Gating. *J Neurosci* **33**:11253–11261. DOI:10.1523/JNEUROSCI.0620-13.2013

579 Sweet T-B, Cox DH. 2008. Measurements of the BKCa channel's high-affinity Ca2+
580 binding constants: effects of membrane voltage. *J Gen Physiol* **132**:491–505.
581 DOI:10.1085/jgp.200810094
582 Tao X, Hite RK, MacKinnon R. 2017. Cryo-EM structure of the open high-conductance
583 Ca2+-activated K+ channel. *Nature* **541**:46–51. DOI:10.1038/nature20608
584 Wu Y, Yang Y, Ye S, Jiang Y. 2010. Structure of the gating ring from the human large-
585 conductance Ca2+-gated K+ channel. *Nature* **466**:393–397.
586 DOI:10.1038/nature09252
587 Xia X-M, Zeng X, Lingle CJ. 2002. Multiple regulatory sites in large-conductance calcium-
588 activated potassium channels. *Nature* **418**:880–884. DOI:10.1038/nature00956
589 Yang H, Hu L, Shi J, Delaloye K, Horrigan FT, Cui J. 2007. Mg2+ mediates interaction
590 between the voltage sensor and cytosolic domain to activate BK channels. *Proc Natl*
591 *Acad Sci USA* **104**:18270–5. DOI:10.1073/pnas.0705873104
592 Yang H, Shi J, Zhang G, Yang J, Delaloye K, Cui J. 2008. Activation of Slo1 BK channels
593 by Mg2+ coordinated between the voltage sensor and RCK1 domains. *Nat Struct Mol*
594 *Biol* **15**:1152–1159. DOI:10.1038/nsmb.1507
595 Yang H, Zhang G, Cui J. 2015. BK channels: multiple sensors, one activation gate. *Front*
596 *Physiol* **6**:1–16. DOI:10.3389/fphys.2015.00029
597 Yang J, Krishnamoorthy G, Saxena A, Zhang G, Shi J, Yang H, Delaloye K, Sept D, Cui
598 J. 2010. An Epilepsy/Dyskinesia-Associated Mutation Enhances BK Channel
599 Activation by Potentiating Ca2+ Sensing. *Neuron* **66**:871–883.
600 DOI:10.1016/j.neuron.2010.05.009
601 Ye S, Li Y, Chen L, Jiang Y. 2006. Crystal Structures of a Ligand-free MthK Gating Ring:
602 Insights into the Ligand Gating Mechanism of K+ Channels. *Cell* **126**:1161–1173.
603 DOI:10.1016/j.cell.2006.08.029
604 Yuan P, Leonetti MD, Pico AR, Hsiung Y, MacKinnon R. 2010. Structure of the Human

605 BK Channel Ca2+-Activation Apparatus at 3.0 Å Resolution. *Science (80-)* **329**:182–
606 186. DOI:10.1126/science.1190414.Structure
607 Yuan P, Leonetti MD, Hsiung Y, MacKinnon R. 2012. Open structure of the Ca2+ gating
608 ring in the high-conductance Ca2+-activated K+ channel. *Nature* **481**:94–97.
609 DOI:10.1038/nature10670
610 Zeng X-H, Xia X-M, Lingle CJ. 2005. Divalent Cation Sensitivity of BK Channel Activation
611 Supports the Existence of Three Distinct Binding Sites. *J Gen Physiol* **125**:273–286.
612 DOI:10.1085/jgp.200409239
613 Zhang G, Huang S-Y, Yang J, Shi J, Yang X, Moller A, Zou X, Cui J. 2010. Ion sensing in
614 the RCK1 domain of BK channels. *Proc Natl Acad Sci USA* **107**:18700–18705.
615 DOI:10.1073/pnas.1010124107
616 Zhang G, Geng Y, Jin Y, Shi J, McFarland K, Magleby KL, Salkoff L, Cui J. 2017. Deletion
617 of cytosolic gating ring decreases gate and voltage sensor coupling in BK channels.
618 *J Gen Physiol* **149**:373–387.
619 Zhou Y, Zeng X-H, Lingle CJ. 2012. Barium ions selectively activate BK channels via the
620 Ca2+-bowl site. *Proc Natl Acad Sci USA* **109**:11413–11418.
621 DOI:10.1073/pnas.1204444109
622 Zhou Y, Yang H, Cui J, Lingle CJ. 2017. Threading the biophysics of mammalian Slo1
623 channels onto structures of an invertebrate Slo1 channel. *J Gen Physiol* **149**:985–
624 1007. DOI:10.1085/jgp.201711845
625

Acknowledgments

We thank Mrs. Luisa Soto (University of Valparaiso) for excellent technical assistance. This research was supported by FONDECYT Grant No. 1150273 and AFOSR No. FA9550-16-1- 0384 to R.L.; CONICYT-PFCHA Doctoral fellowships to Y.L.C.; FONDECYT Grant No. 1180999 to K.C. The Centro Interdisciplinario de Neurociencia de Valparaiso is a Millennium Institute supported by the Millennium Scientific Initiative of the Chilean Ministry of Economy, Development, and Tourism (P029-022-F).

Competing interests

The authors declare no competing financial interests.

636 **Figures**

637 **Figure 1.**

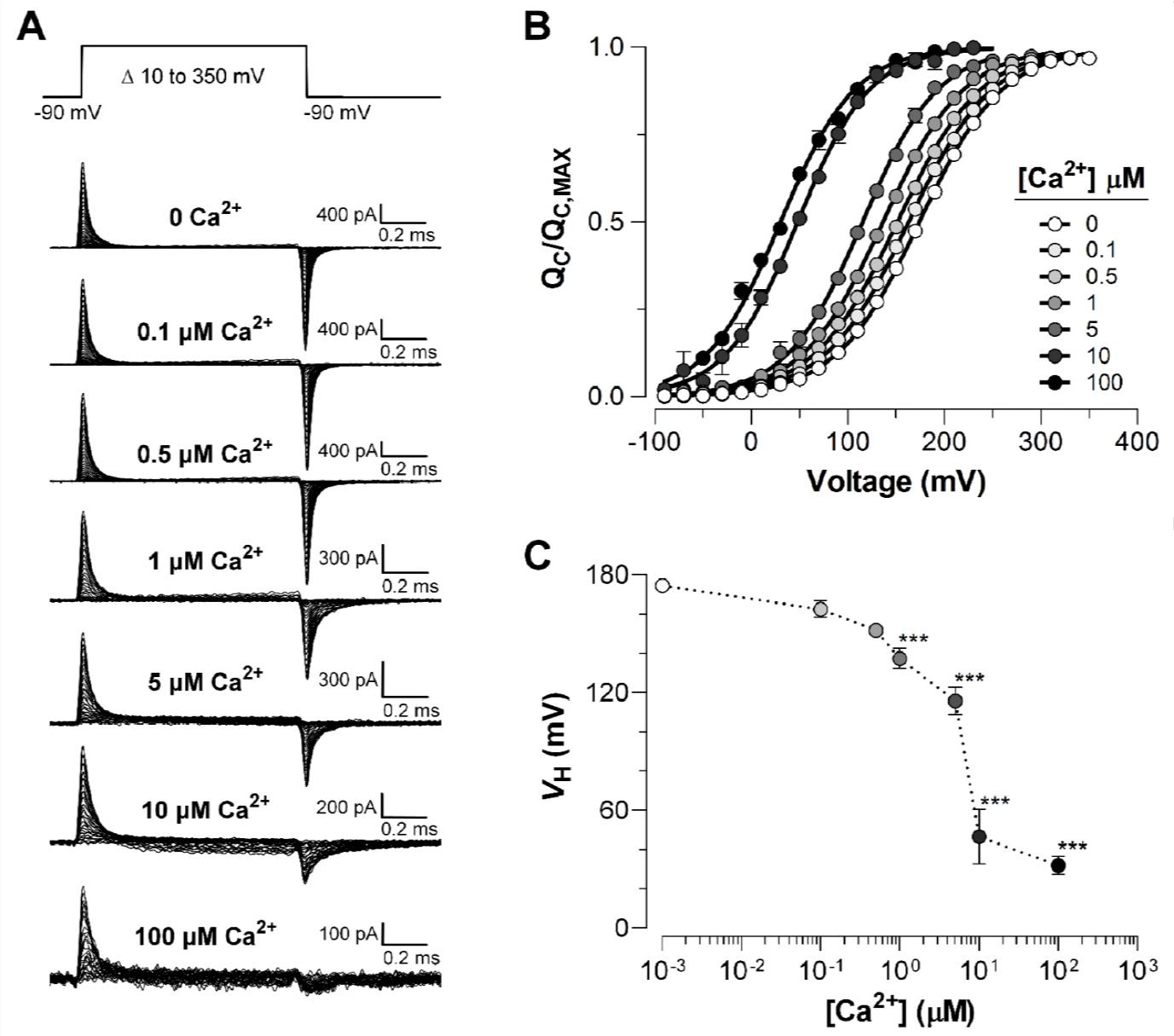

638

639 **Figure 2.**

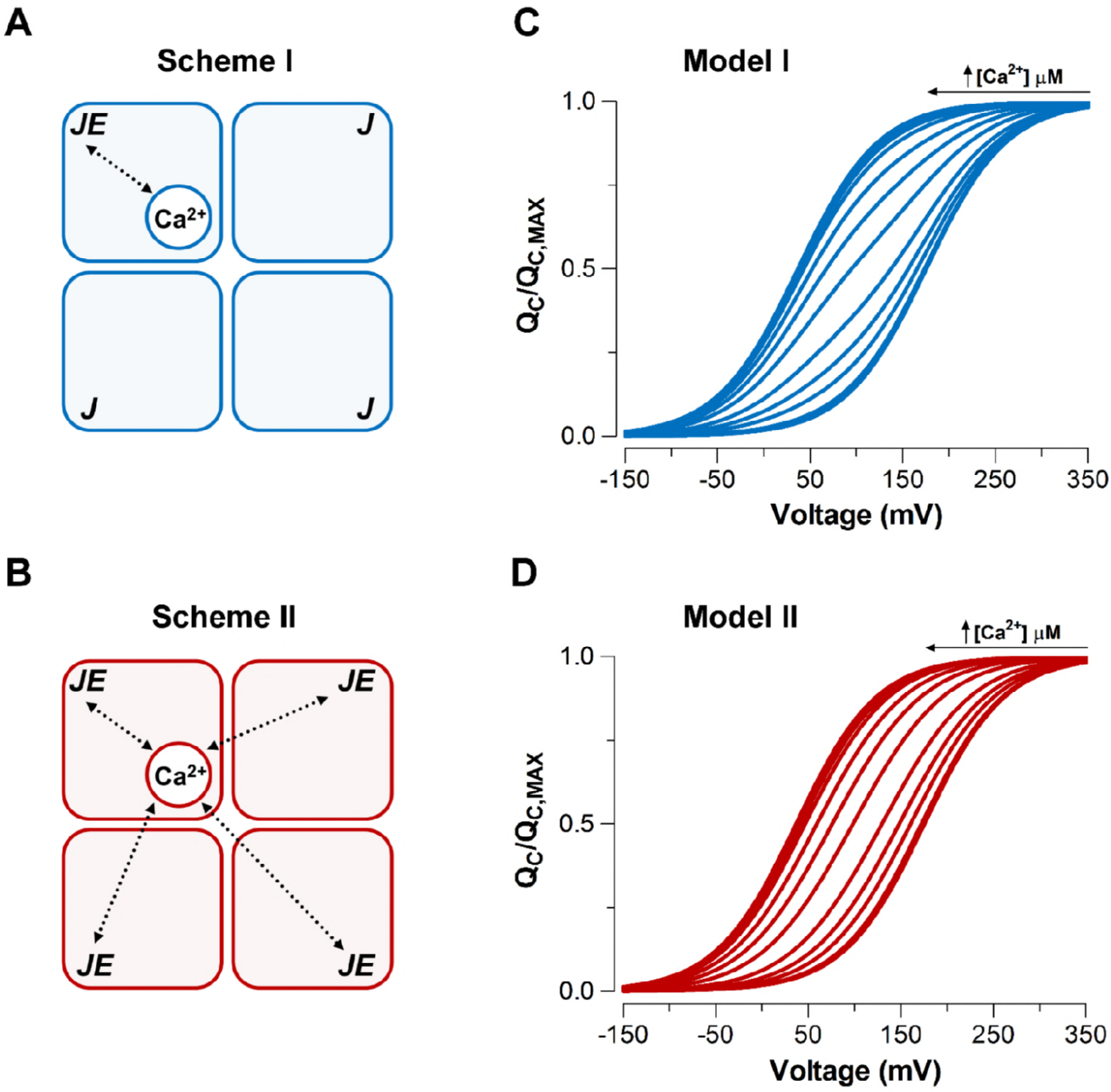

640

641 **Figure 3.**

642

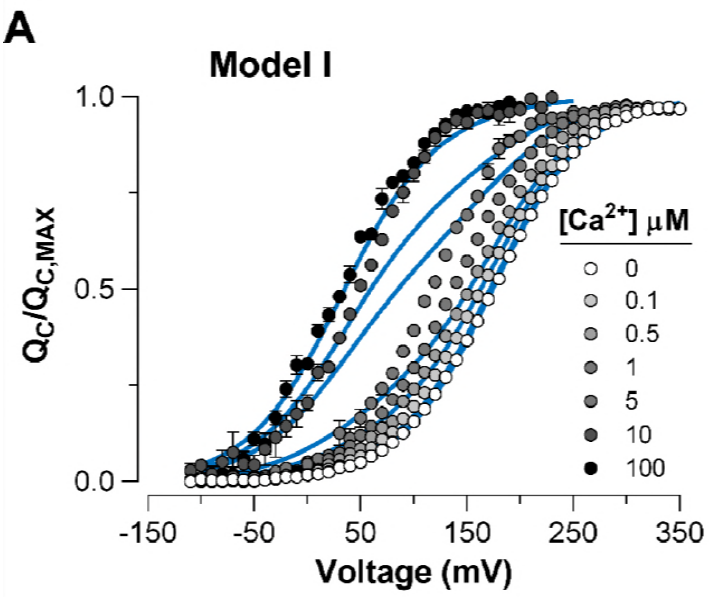

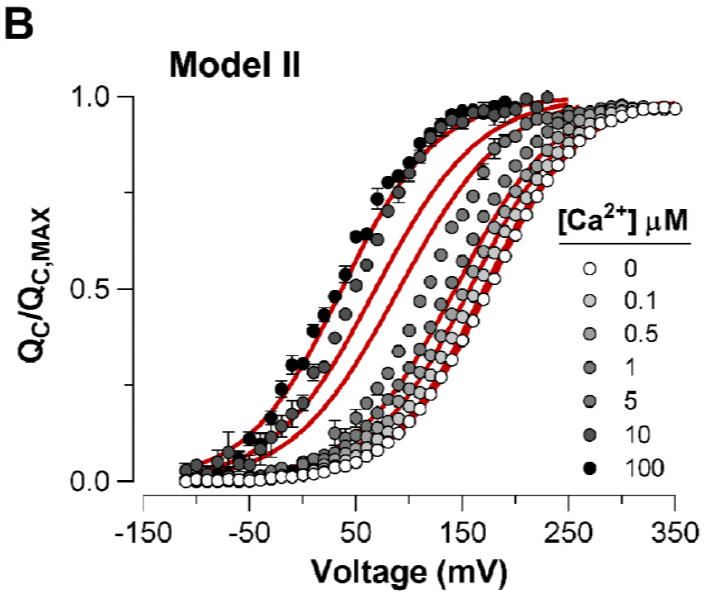

C

Model Parameters	Model I	Model II
z_J	0.58	0.58
J_0	0.018	0.018
E_M	26.4*	2.27*
K_D (µM)	3.9	4.3
AIC	-784.1	-946.5

* Fixed parameters in the model fitting. AIC values correspond to Akaike Information Criterion to select the best fit model.

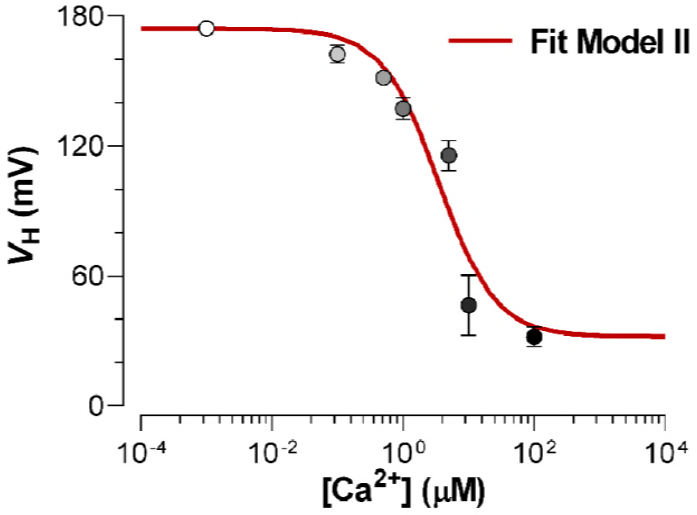

643 **Figure 4.**

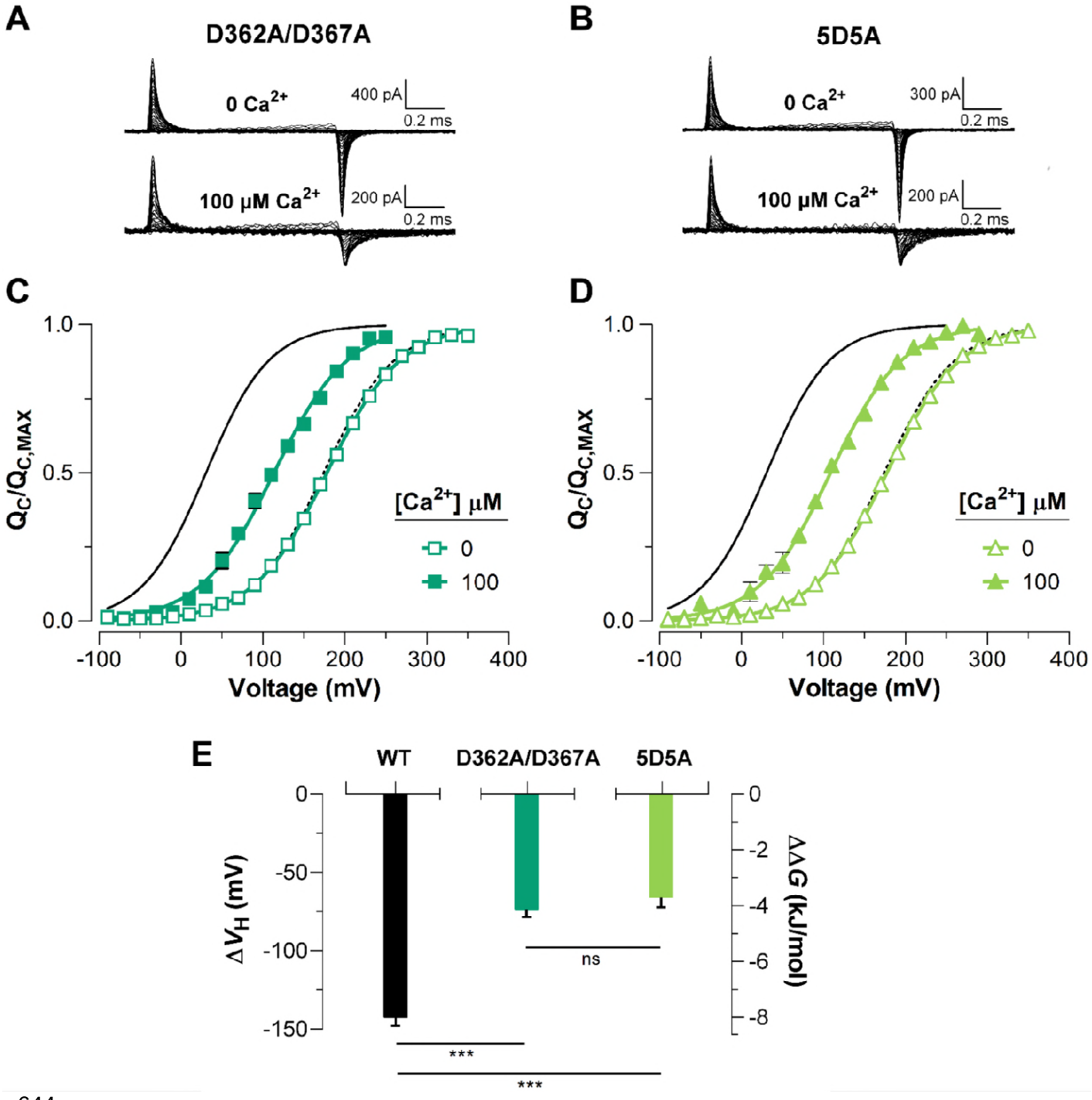

644

645 **Figure 5.**

646

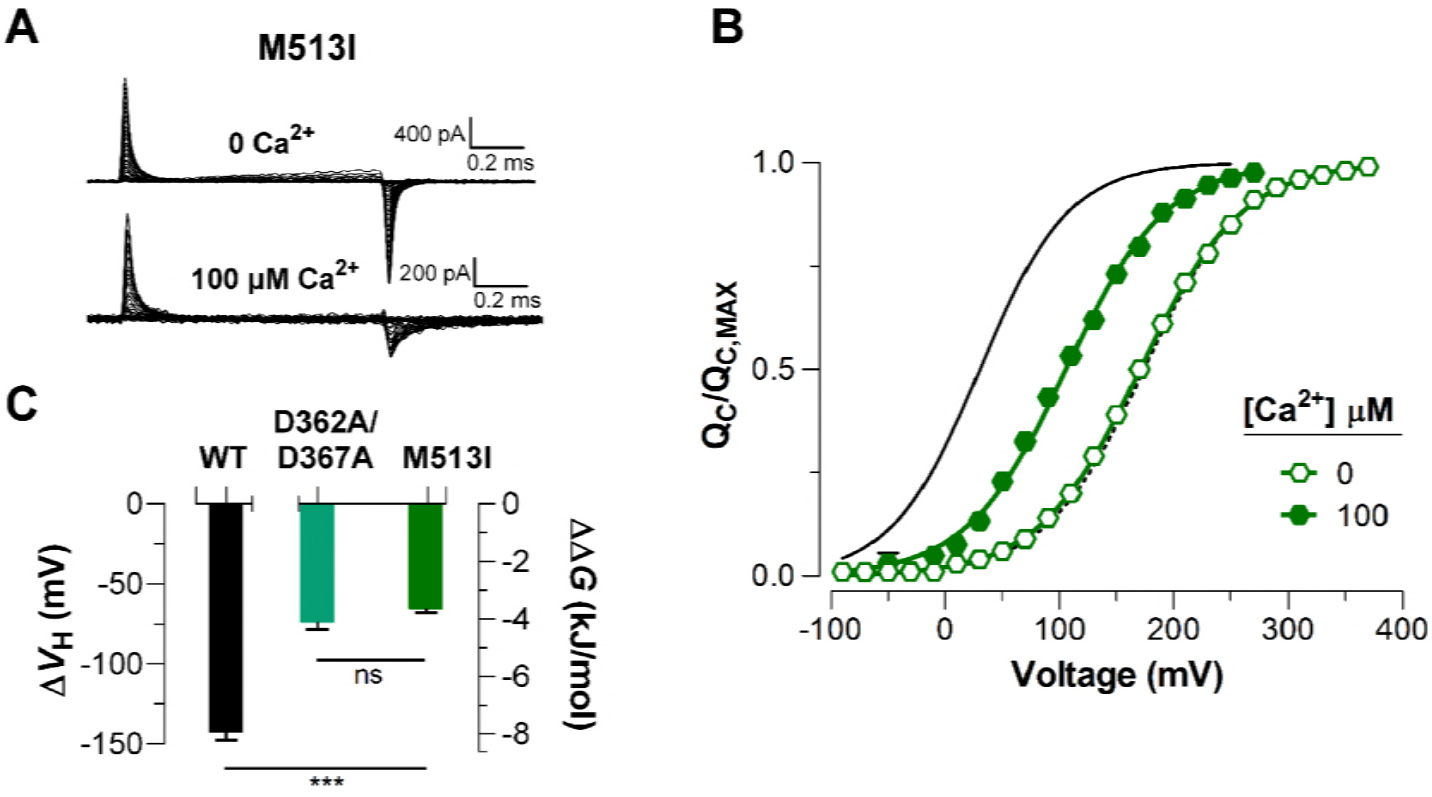

Tables

Table 1. Parameters for the extended Ca^{2+}-VSD interaction model (Model II) including two high-affinity Ca^{2+}-binding sites per α-subunit.

	Model II	
Model Parameters	With cooperativity	Without cooperativity
z_J	0.58	0.59
J_0	0.018	0.018
E_{S1}	1.46*	
E_{S2}	1.52*	
K_{D1} (μM)	15.6	3.9
K_{D2} (μM)	1.9	2.8
G	2.6	1*
AIC	-949.9	-947.8

* Fixed parameters in the model fitting. AIC values correspond to Akaike Information Criterion to select the best fit model.

Legends Figures

Figure 1. Effects of Ca^{2+}-binding on VSD activation in BK channels. (**A**) Representative gating current (I_G) recordings at different internal Ca^{2+} concentrations (from 0 to 100 µM). I_G were evoked by the indicated voltage protocol of 1 ms duration. (**B**) Gating charge-voltage relationships ($Q_C(V)$) were obtained by integrating the fast component for each ON I_G trace. Normalized gating charge data $\left(Q_C(V)/Q_{C,\ MAX}\right)$ (mean ± SEM) were fitted using a single Boltzmann function (solid lines). (**C**) V_H obtained from the $Q_C(V)$ curves as a function of Ca^{2+} concentration (mean ± SEM). At zero" Ca^{2+} condition $V_{H\,(0\ Ca^{2+})}$ = 174.5 ± 2.4 mV (n = 25), whereas Ca^{2+} binding produce a leftward shift in V_H (ΔV_H): 0.1 µM Ca^{2+} (ΔV_H = -12.1 ± 3.5 mV, n = 5); 0.5 µM Ca^{2+} (ΔV_H = -22.9 ± 1.8 mV, n = 5); 1 µM Ca^{2+} (ΔV_H = -37.1 ± 3.5 mV, n = 5); 5 µM Ca^{2+} (ΔV_H = -58.8 ± 6.7 mV, n = 6); 10 µM Ca^{2+} (ΔV_H = -127.9 ± 13.9 mV, n = 6); 100 µM Ca^{2+} (ΔV_H = -142.6 ± 4.5 mV, n = 7). The one-way ANOVA followed by Dunnett's post-hoc test analysis was used to assess statistical significance of the Ca^{2+}-induced shifts in V_H (***p< 0.001).

Figure 2. Model-dependent behavior of the $Q_C(V)$ curves based on the CTD-VSD interaction mechanisms according to the fractional occupancy of Ca^{2+}-binding sites. (**A-B**) Cartoons representing two interaction schemes between voltage sensors and Ca^{2+}-binding sites (modify from Horrigan and Aldrich (2002)). The Scheme I (**A**) assume that Ca^{2+}-binding only affects the voltage sensor of one α-subunit (E_{M1}). The Scheme II (**B**) predicts that binding of Ca^{2+} to one α-subunit affects VSD in all subunits equally, increasing the voltage sensor equilibrium constants (J) E_{M2}-fold in all four subunits (E_{M2}^4, when the four Ca^{2+} sites are occupied). In both schemes, a single Ca^{2+}-binding site is considered in each

673 α-subunit. (**C-D**) Predictions of $Q_C(V)$ relationships at different internal calcium
674 concentration (from 0 to 10 mM) by two distinctive interaction mechanisms between Ca^{2+}-
675 binding sites and voltage sensors (Scheme I and Scheme II), respectively. $Q_C(V)$ curves
676 were generated using Equation 4 (blue: Model I) or Equation 6 (red: Model II), and the
677 following set of parameters: z_J = 0.58, J_0 = 0.018, K_D = 11 μM and $E_{M1} = E_{M2}^4$ = 25.

678 **Figure 3. Dose-dependent effect of Ca^{2+} on voltage sensor activation is predicted by**
679 **a Ca^{2+}-VSD interaction mechanism defining that Ca^{2+}-binding equally affects the VSD**
680 **in all four α-subunits.** (**A-B**) The experimental $Q_C(V)$ data were fitted with the two possible
681 allosteric interaction mechanisms between voltage and calcium sensors described by the
682 Scheme I and Scheme II. The blue and red lines represent the global fits by Model I and
683 Model II, respectively. The allosteric factor E (E_{M1} and E_{M2}) was constrained to the value
684 obtained from the individual fitting of the $Q_C(V)/Q_{C,\ MAX}$ curves at 0 and 100 μM Ca^{2+}
685 (experimental E (E_{exp}) equal to 26.4). The z_J, J_0 and K_D parameters were allowed to vary
686 freely. (**C**) Parameters for the best fits of the $Q_C(V)$ data. Note that the allosteric factor E
687 for Model I (E_{M1}) and Model II (E_{M2}) have different interpretations, being $E_{M2} = E_{exp}$
688 whereas $E_{M2} = \sqrt[4]{E_{exp}}$ given that the four voltage sensor will be altered in 2.3-fold (E_{M2} =
689 2.27) with each additional Ca^{2+} bound. Based on the Akaike Information Criterion (AIC), the
690 best model fit to the $Q_C(V, [Ca^{2+}])$ data is achieved using the Ca^{2+}-VSD interaction scheme
691 described by Model II. (**D**) The Ca^{2+}-dependence of V_H-$Q_C(V)$ curves are superimposed
692 with the predicted V_H by Model II (red line).

693 **Figure 4. The high-affinity Ca^{2+}-binding sites contribute equally to allosteric coupling**
694 **between calcium and voltage sensors in BK channels.** (**A-B**) Representative gating

current (I_G) recordings at 0 and 100 μM of $[Ca^{2+}]_i$ for the RCK1 site mutant (D362A/D367A) and the RCK2 site mutant (5D5A), respectively. (**C-D**) Gating charge-voltage curves ($Q_C(V)$) were obtained at 0 Ca^{2+} (open symbols) and 100 μM Ca^{2+} (filled symbols) for D362A/D367A and 5D5A mutants, respectively. Boltzmann fitting to the experimental data (mean ± SEM) is indicated by solid lines ($V_{H(D362A/D367A)}$ = 178.0 ± 2.7 mV, n = 12 and $V_{H(5D5A)}$ = 176.4 ± 4.6 mV, n = 17 at "zero" Ca^{2+}; $V_{H(D362A/D367A)}$ = 104.2 ± 7.3 mV, n = 7 and $V_{H(5D5A)}$ = 110.8 ± 6.7 mV, n = 6 at 100 μM Ca^{2+}). For comparison, all $Q_C(V)$ plots include the Boltzmann fit of the $Q_C(V)$ curves for WT at 0 Ca^{2+} (dashed black line) and 100 μM Ca^{2+} (solid black line). (**e**) Quantification of the V_H shift (ΔV_H) in the $Q_C(V)$ curves and the free energy change ($\Delta\Delta G_V^{Ca}$) induced by 100 μM Ca^{2+}. The non-parametric *t*-test was used to evaluate statistical significances between WT BK channel and the RCK sites mutants (***p<0.001; ns: non-significant).

Figure 5. Mutations abolishing Ca^{2+}-sensing by the RCK1 binding-site reduce the Ca^{2+}-induced effect on voltage sensors activation similarly. (**A**) Representative gating current (I_G) recordings at 0 and 100 μM of $[Ca^{2+}]_i$ for the RCK1 site mutant M513I. (**B**) Gating charge-voltage curves $Q_C(V)$ were obtained at 0 Ca^{2+} and 100 μM Ca^{2+} (open and filled symbols) for the M513I mutant. Boltzmann fitting to the experimental data (mean ± SEM) is indicated by solid lines ($V_{H(M513I)}$ = 170.4 ± 4.4 mV, n = 17 at "zero" Ca^{2+} and $V_{H(M513I)}$ = 105.0 ± 6.3 mV, n = 4 at 100 μM Ca^{2+}). For comparison, the $Q_C(V)$ plot includes the Boltzmann fit of the $Q_C(V)$ curves for WT at 0 Ca^{2+} and 100 μM Ca^{2+} (dashed and solid black line). (**C**) Quantification of the V_H (ΔV_H) shift in the $Q_C(V)$ curves and the free energy change induced by 100 μM Ca^{2+} ($\Delta\Delta G_V^{Ca}$). The non-parametric t-test was used to compare

717 statistical significances between WT BK channel and the RCK1-site mutants (***p<0.001;

718 ns: non-significant).

Supplementary Information

Assumptions and model predictions. We assume that the four voltage sensors act independently transiting between two states, resting (R) and active (A), governed by the voltage-dependent equilibrium constant J. The R–A equilibrium is displaced toward the active state by membrane depolarization generating a fast gating charge movement (Q_C) before channels opening. Additionally, the Ca^{2+}-binding to high-affinity sites shifts the voltage sensor equilibrium toward their active configuration through an allosteric coupling described by the factor E (***Figure 2—figure supplement 1A***). By assuming the simplified standard model for the BK channels (Horrigan and Aldrich, 2002), where each α-subunit has a single Ca^{2+}-binding site, we established the possible states and their connections through which each voltage sensor transit in presence of Ca^{2+} (***Figure 2—figure supplement 1B;C***) following the CTD-VSD interaction mechanisms described by the Scheme I and Scheme II (***Figure 2A,B***).

For Scheme I, in which Ca^{2+}-binding sites and voltage sensors can only interact within the same α-subunit, the activation of each VSD can occur through the R_0-A_0 or R_1-A_1 transitions according to the functional state of the Ca^{2+} site (unbound or Ca^{2+} bound). The equilibrium of such transitions is governed by J or JE_{M1}, respectively (***Figure 2—figure supplement 2B***). In the case of Scheme II, in which binding of Ca^{2+} to a single α-subunit affects the four voltage sensors equally, the R-A equilibrium of each VSD would be affected by the number of Ca^{2+} bound in the channel (0-4) depicted in the model (Model II) as five possible R-A transitions. According to this model, the J constant increase E_{M2}-fold for each occupied Ca^{2+} site (***Figure 2—figure supplement 1C***). For both schemes, the horizontal transitions R-R and A-A represent the Ca^{2+}-binding equilibrium (K or KE) when the VSD is in the resting or

742 active conformation, respectively. The K equilibrium constant is defined as the
743 bound/unbound probability ratio for each Ca^{2+}-binding site and depends on Ca^{2+}
744 concentration ($[Ca^{2+}]$) and the Ca^{2+} dissociation constant (K_D): $K = [Ca^{2+}]/K_D$.

745 Here, we assume that the voltage sensor movement at ON-gating currents is in equilibrium
746 relative to the binding of Ca^{2+}. The assumption is reasonable since the Ca^{2+}-binding rate
747 constant estimated for BK channel is about 10^8 $M^{-1}s^{-1}$ (Hou et al., 2016) implying that at 10
748 μM internal Ca^{2+} the association time constant is 1 ms. Thus, Ca^{2+} binding at this Ca^{2+}
749 concentration proceeds at a pace about 33-fold slower than the voltage sensor movement
750 (~30 μs). Based on this consideration, the R-A transitions in the models would be
751 predominant transitions whose proportion will be determined by the $[Ca^{2+}]$ and K_D.
752 Therefore, predictions of the $Q_C(V)$ curves at different Ca^{2+} concentrations for Model I and
753 Model II were based on a given fractional occupancy of Ca^{2+} sites established by the
754 probability of Ca^{2+} bound (b) and unbound $(1-b)$ for each Ca^{2+}-sensor, and the energetic
755 contribution to VSD equilibrium.

756 Simulations of the $Q_C(V)$ curves using the Scheme I (Model I) were obtained using the
757 equation

758 $$\frac{Q_C(V)}{Q_{C,\ MAX}} = (1-b)\left(\frac{1}{1+J^{-1}}\right) + b\left(\frac{1}{1+(JE_{M1})^{-1}}\right) \qquad (1);$$

759 where

760 $$b = \frac{1}{1+K^{-1}} = \frac{1}{1+\frac{K_D}{[Ca^{2+}]}} = \frac{[Ca^{2+}]}{[Ca^{2+}]+K_D} \qquad (2);$$

761 and

762 $$J = J_0 e^{\frac{z_J FV}{RT}} \quad (3)$$

763 Substituting b and J into Equation (1), the Ca^{2+}-dependent voltage sensor activation for

764 Model I is given by the equation

765 $$\frac{Q_C(V)}{Q_{C,\ MAX}} = \left(\frac{K_D}{[Ca^{2+}] + K_D}\right)\left(\frac{1}{1 + \frac{e^{\frac{-z_J FV}{RT}}}{J_0}}\right) + \left(\frac{[Ca^{2+}]}{[Ca^{2+}] + K_D}\right)\left(\frac{1}{1 + \frac{e^{\frac{-z_J FV}{RT}}}{J_0 E_{M1}}}\right) \quad (4)$$

766 Thus, the $Q_C(V)$ curves are determined by the proportion of two functional VSD populations

767 with a distinctive effect (unliganded effect or Ca^{2+}-saturated effect) Consequently, the

768 $Q_C(V)$ curves are represented by a weighted sum of two Boltzmann functions.

769 Meanwhile, for the concerted CTD-VSD interaction Scheme II (Model II), the $Q_C(V, [Ca^{2+}])$

770 curves would be determined using the general equation:

771 $$\frac{Q_C(V)}{Q_{C,\ MAX}} = \sum_{x=0}^{n} \binom{n}{x} (1-b)^{n-x} b^x \left(\frac{1}{1 + (JE_{M2}^x)^{-1}}\right) \quad (5)$$

772 The expression in the first bracket represents the fraction of VSD belonging to a channel

773 with x (0 to 4) Ca^{2+} bound, according to a binomial probability distribution. Thus, the $Q_C(V)$

774 curves result in a weighted sum of five distinct Boltzmann functions corresponding to the

775 five possible R-A transitions (***Figure 2—figure supplement 1C***). By stating $n = 4$ because

776 the tetrameric symmetry of the channels, and substituting b and J into the previous equation

777 (Equation 5) we have

$$\frac{Q_{\mathrm{C}}(V)}{Q_{\mathrm{C,\ MAX}}} = \sum_{x=0}^{4} \binom{4}{x} \left(\frac{K_D}{[Ca^{2+}] + K_D}\right)^{4-x} \left(\frac{[Ca^{2+}]}{[Ca^{2+}] + K_D}\right)^{x} \left(\frac{1}{1 + \frac{e^{\frac{-z_J FV}{RT}}}{J_0 E_{M2}^{x}}}\right) \quad (6)$$

It should be noted that at limiting Ca^{2+} conditions, both schemes become equivalent where the VSD activation is characterized by a single Boltzmann function. At zero Ca^{2+}, the $Q_{\mathrm{C}}(V)$ curves are described by

$$\frac{Q_{\mathrm{C}}(V)}{Q_{\mathrm{C,\ MAX}}} = \left(\frac{1}{1 + \frac{e^{\frac{-z_J FV}{RT}}}{J_0}}\right),$$

whereas Ca^{2+} saturating concentration J is multiply by the allosteric factor E, where $E = E_{M1} = E_{M2}^{4}$ depending on the model (Model I or Model II):

$$\frac{Q_{\mathrm{C}}(V)}{Q_{\mathrm{C,\ MAX}}} = \left(\frac{1}{1 + \frac{e^{\frac{-z_J FV}{RT}}}{J_0 E}}\right)$$

Given that each α-subunit has two Ca^{2+}-binding sites, we expanded the CTD-VSD interaction Scheme II (***Figure 2—figure supplement 1C***) considering the existence of two Ca^{2+}-binding sites (***Figure 2—figure supplement 1D,E***). The Model II includes the energetic contribution of RCK1 and RCK2 Ca^{2+}-sites to the VSD activation. The factor $E = E_{S1} * E_{S2}$ where E_{S1} and E_{S1} are the allosteric coupling between the VSD and the RCK1 Ca^{2+}-site and RCK2 Ca^{2+}-site, respectively. The K_1 and K_2 constants define the bound/unbound transition for each RCK1 and RCK2 sites being $K_1 = [Ca^{2+}]/\ K_{D1}$ and

$K_2 = [Ca^{2+}]/\ K_{D2}$. Assuming that the Ca^{2+} sensors of distinct α-subunit do not interact, we only consider intrasubunit cooperativity between the RCK1 and RCK2 sites defined by the factor G. Thus, the occupancy of one RCK site will affect Ca^{2+}-binding equilibrium to the other RCK site in the α-subunit (GK_1 and GK_2) (***Figure 2—figure supplement 1E***). The equilibrium J of the VSD increase E_{S1}-fold and E_{S2}-fold for the each Ca^{2+} bound to RCK1 and RCK2 sites, respectively, reaching to $JE_{S1}^4E_{S2}^4$ when the eight Ca^{2+} sites are occupied.

Supplementary Figures

Figure 1—figure supplement 1.

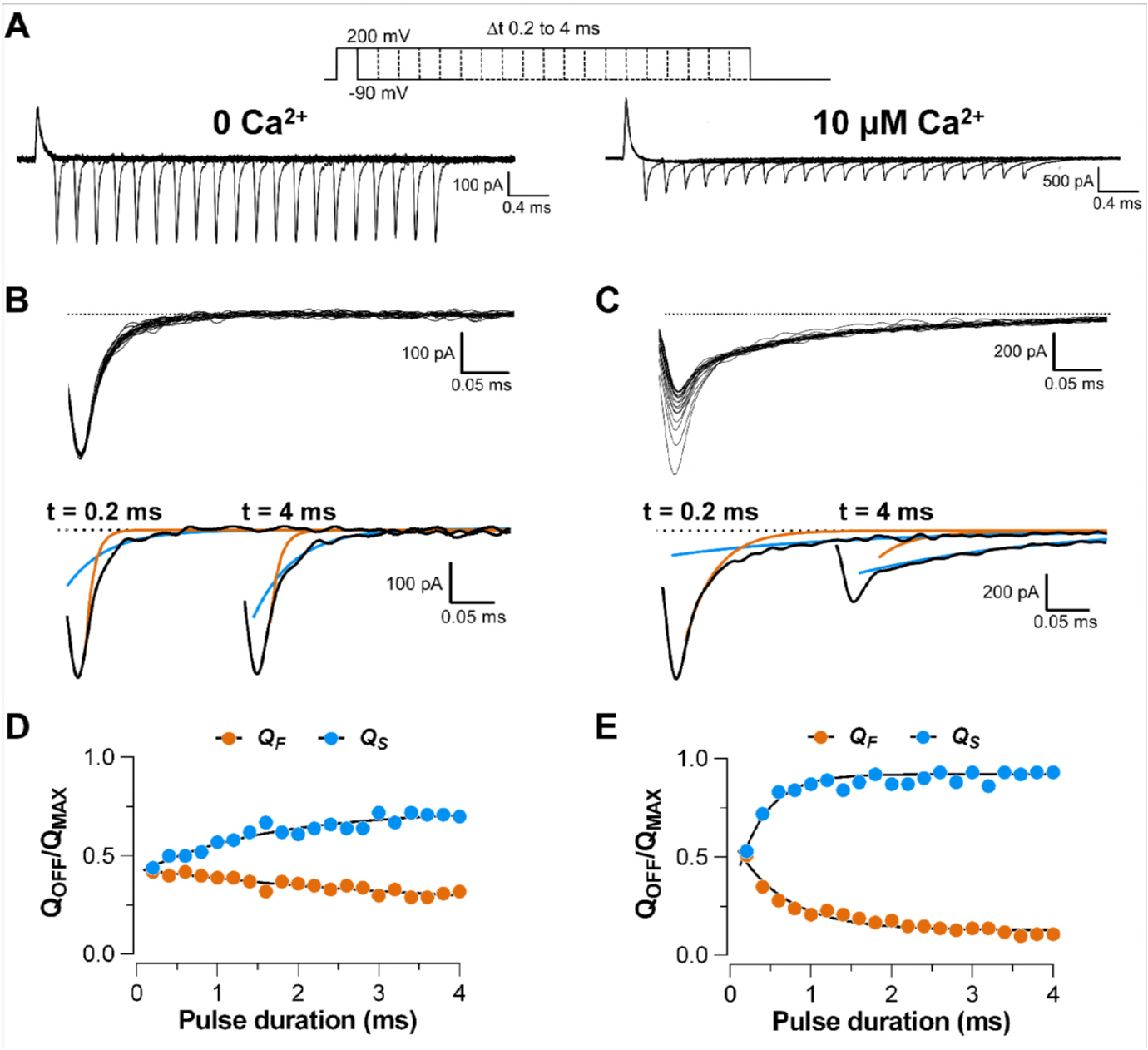

802 **Figure 2—figure supplement 1.**

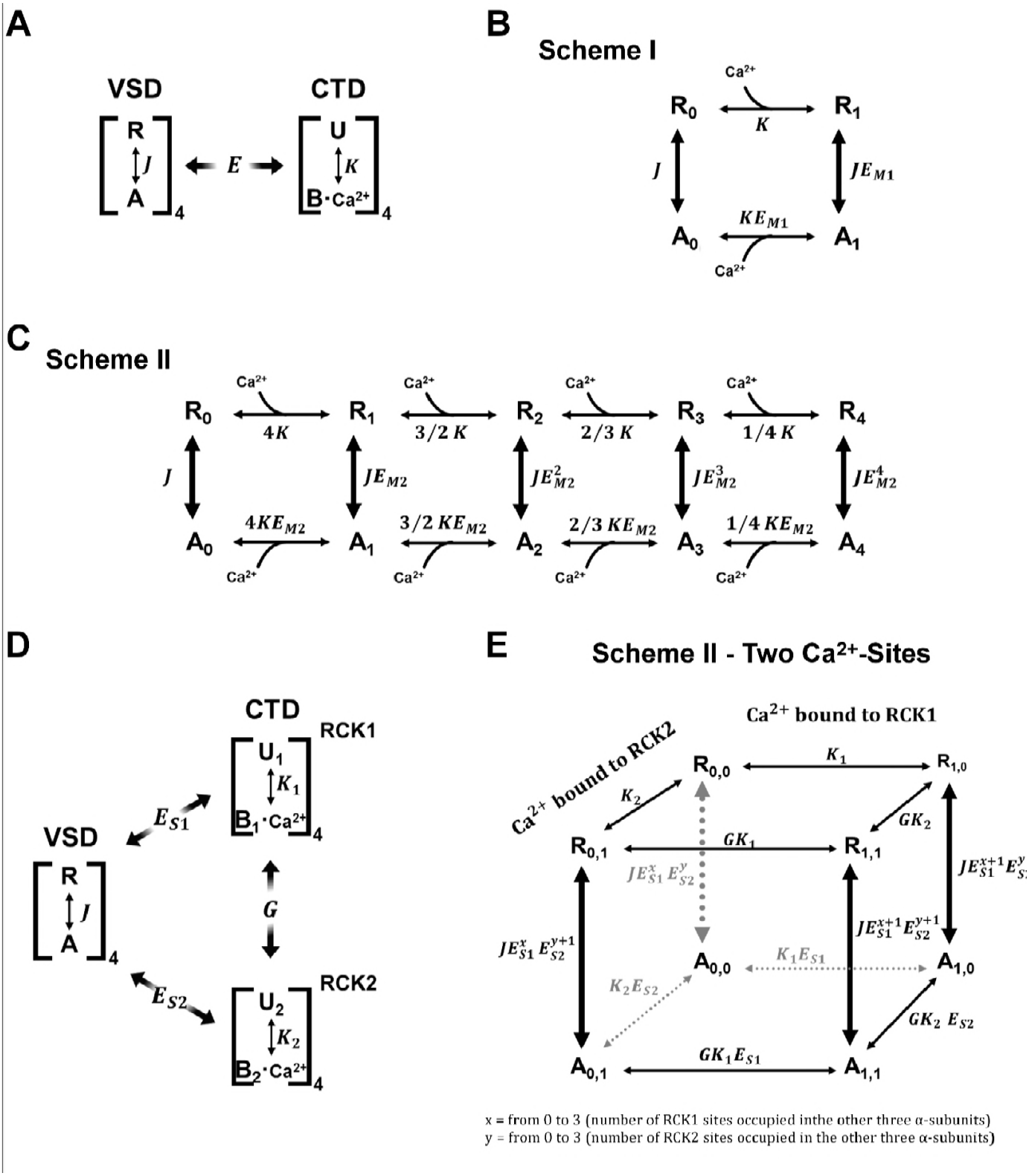

803

Legends Supplementary Figures

Figure 1—figure supplement 1. Ca^{2+} increase the slow component of the OFF gating currents. (**A**) Gating current (I_G) recordings evoked by 200 mV pulses with different durations (from 0.2 to 4 ms) at 0 and 10 μM [Ca^{2+}] conditions, respectively. (**B-C**) The top panels show the superimposed traces of the I_G-OFF recorded at -90 mV evidencing a decrease in amplitude and a slower decay of the OFF current as the duration of the pulse increases at 10 μM Ca^{2+}. The dashed line represents the baseline for each experiment. I_G-OFF were fitted with an exponential function of two-components (fast and slow components). I_G-OFF traces at 0.2 ms and 4 ms pulse duration are displayed for each Ca^{2+} condition. Orange and blue lines correspond to fast and slow components of the two-exponential fits, respectively: (**B**) "zero" Ca^{2+} (τ_F = 10 μs and τ_S= 44 μs) and (C) 10 μM Ca^{2+} (τ_F = 25 μs and τ_S = 212 μs). (**D-E**) The relative amplitude of the OFF-charge components, the fast (Q_F) and slow (Q_S) charge components were plotted against the pulse duration and fitted with an exponential function representing the time course of the opening of the channel: (**D**) "zero" Ca^{2+} ($\tau_{0Ca^{2+}}$ = 1.8 ms) and (**E**) 10 μM Ca^{2+} ($\tau_{10\ \mu M}$ = 536 μs).

Figure 2—figure supplement 1. Kinetic models of the VSD activation according to the CTD-VSD interaction schemes. (**A**) Sub-scheme describing calcium and voltage allosteric interaction for closed channels. The VSD transit between two resting (R) and active (A) configuration governed by the equilibrium constant J, whereas each Ca^{2+} site undergoes unbound (U) - Ca^{2+} bound (B) transitions governed by the equilibrium constant K. The allosteric factor E accounts for the coupling between the calcium and voltage sensors (CTD-VSD) (**B-C**) VSD kinetic models in presence of Ca^{2+} according to CTD-VSD interaction schemes I and II (***Figure 2A,B***), respectively, where the vertical transitions (R-A) represent

the VSD movement and the horizontal transitions (R-R and A-A) are Ca^{2+}-binding reactions when the VSD is in the resting or active conformation. For the Scheme I (**B**), each VSD can undergo R_0-A_0 or R_1-A_1 transitions depending on the unbound or bound state of the Ca^{2+} site in the α-subunit, respectively. Thus, the R_1-A_1 equilibrium is defined by J increased E_{M1}-fold (JE_{M1}). For the Scheme II (**C**), the R_0-A_0 to R_4-A_4 transitions represent the VSD equilibrium with 0, 1, 2, 3, and 4 occupied Ca^{2+} sites in the channel. Thus, for each Ca^{2+} bound the equilibrium constant J increase E_{M2}-fold reaching to JE_{M2}^4 when the four Ca^{2+} sites are occupied. The thickness of the arrows indicates the probability of transitions. (**D**) General sub-scheme of the CTD-VSD interaction including two Ca^{2+} sites for each CTD (RCK1 and RCK2 sites). For each RCK1 and RCK2 site the unbound-Ca^{2+} bound transitions are governed by the equilibrium constants K_1 and K_2. The factor G describe the cooperativity between the sites within the same α-subunit; and the E_{S1} and E_{S2} factors define the allosteric coupling between the RCK1 and RCK2 sites and the VSD, respectively. (**E**) Schematic representation of VSD kinetic model according to the extended version of the Scheme II (**C**) accounting for both RCK1 and RCK2 Ca^{2+}-sites on each α-subunit. For sake of simplicity, are only depicted the VSD transitions depending on the unbound or bound state of the RCK sites within the same α-subunit: RCK1 site ($R_{1,0}$-$A_{1,0}$), RCK2 site ($R_{0,1}$-$A_{0,1}$) and both sites ($R_{1,1}$-$A_{1,1}$).